Abstract

We present results from an all-sky search for gravitational-wave ring-down bursts in the data collected by the LIGO, GEO 600 and Virgo detectors between May and October 2007.

1 Introduction

Compact stars, when excited, are expected to emit gravitational waves at their kilo-Hertz f-mode frequencies and sub-second damping times. For example, during pulsar glitches, magnetar flares, such damped oscillations (usually referred to as ring-downs) are thought to be triggered. Also, newly formed compact stars, may suffer phase transitions, from hadronic to quark matter, as a result of spindown and/or cooling. Or, accretion in low-mass x-ray binaries (LMXBs) may result in a density increase which can -in turn- trigger large-scale mass rearrangements and cause strong gravitational-wave (GW) emission. Compact binary mergers with low-mass components may lead to formation of compact stars as well (instead of promptly forming black holes) which wildly pulsate at their f-mode frequencies and emit considerable amounts of gravitational radiation.

Various searches for GWs from neutron-star f-mode ring-downs were contacted during the past few years. Most of them were in coincidence with electromagnetic triggers from magnetars [16, 17, 20, 22]. Another search was motivated by a timing glitch of the Vela pulsar [18]. Un-modeled all-sky burst searches are also capable of detecting such signals [19]. Because of their general character, though, these searches are less sensitive and they can miss weak, signals hidden in the detector's noise. The high frequencies of the fundamental modes of compact stars [4, 6] make their detection very difficult with first-generation gravitational-wave interferometers. If energy E is emitted in gravitational waves of frequency f_0 from a source at a distance r_0, a signal of strength h_{rss} reaches the earth, where:

$$E = \frac{\pi^2 c^3}{G} r_0^2 f_0^2 h_{rss}^2 \simeq 10^{47} \left(\frac{r_0}{1\text{kpc}} \right)^2 \left(\frac{f_0}{2\text{kHz}} \right)^2 \left(\frac{h_{rss}}{10^{-21}\text{Hz}^{-1/2}} \right)^2 \text{erg} \tag{1}$$

The root-square-sum amplitude h_{rss} is defined by:

$$h_{rss} = \sqrt{\int \left(h_+^2 + h_\times^2 \right) dt} \tag{2}$$

where $h_+ = h_+(t)$, $h_\times = h_\times(t)$ are the plus and cross polarizations of the gravitational wave, respectively. If we assume that we can detect a signal at $f_0 = 2\text{kHz}$ with $h_{rss} = 10^{-21}\text{Hz}^{-1/2}$ at the earth, then we see that, to be sensitive to the whole Galaxy ($r_0 \simeq 10\text{kpc}$), we need a GW energy of about 10^{49}erg. Otherwise, we are sensitive to a local sub-volume of a few or a few hundreds of parsec which makes a detection rather unlikely.

On the theoretical side, there are continuous efforts to understand and describe these phenomena and quantify their astrophysical implications. Among others, the main questions under attack are: how much energy is released and how much of it goes into GWs? what is the form of the emitted signal in terms of frequency, duration, polarization etc? what is the true physical mechanism behind these events? how often they occur? is the observational rate, the true rate? or we are missing (we are not detecting electromagnetically) events which could be possibly detected in gravitational waves?

More than 350 glitches have been observed in more than 100 pulsars, most of them being relatively young, less than 10^8 years old [25, 11, 27]. Glitches are sudden jumps in the pulsars' rotational frequencies usually attributed to crustquakes or crust-core superfluid interactions. It is thought that, during these glitches, amounts of energy are released, possibly proportional to the relative spin-up, $\Delta\Omega/\Omega$. In the crustquake scenarios, if we assume angular momentum conservation, this energy is estimated to be roughly:

$$\Delta E = \frac{1}{2} I \Omega^2 \frac{\Delta\Omega}{\Omega} \simeq 10^{42} \left(\frac{I}{10^{38}\text{kgm}^2} \right) \left(\frac{\Omega}{20\pi\text{rads}^{-1}} \right)^2 \left(\frac{\Delta\Omega/\Omega}{10^{-6}} \right) \text{erg} \tag{3}$$

In glitches involving crust-core superfluid interactions this energy may be considerably lower, of the order of 10^{38}erg. This means that we are sensitive to pulsar glitches happening only in the very vicinity of the earth, in the Local Fluff or the Local Bubble volumes.

On the other hand, it is very likely that we are missing pulsars and/or glitches from known pulsars. The vast majority of pulsars has been discovered because of their radio emission. There could be a large number of pulsars not emitting in radio; the famous "death line" in the $P - \dot{P}$ diagram justifies this suspision. Furthermore, pulsars could be just emitting away from the earth or their emission could be too faint to be detected. Even for the already known and recorded pulsars, there is not a continuous study of their pulsed emission. Timing irregularities can be easily lost.

Since the discovery of magnetars, there have been recorded a few giant flares (approximately one per decade) and many more weaker bursts (hundreds per year). Electromagnetic (flare) emission of magnetars is assumed to be due to these objects' extraordinary magnetic field. The emission is also (as in the case of radio emission of pulsars) assumed to be beamed and so, there could be many more events unseen from our ground- and space-based electromagnetic detectors. The flares are supposed to arise from global rearrangements of the stellar magnetic field. There are many open important questions regarding the emission of these objects in gravitational waves. First of all, is the GW emission as strong as the E/M one? Can the magnetic field reconfiguration cause substantial mass rearrangements?

Then, another important question, is what kind of emission is associated with the flares. Which modes are excited during a flare? What is the frequency and the duration of the emitted waves? In general, basic considerations show that the emissible energy can be large [12, 10]; the excitation of f-modes, however, is questionable [13, 15, 26]; but see also [9]).

Another astrophysical scenario predicting large amounts of gravitational radiation emitted in f-mode frequencies and damping times is that of a phase transition of a young, newly-formed neutron star to a quark compact star. When, after a core collapse, a neutron star is born, it starts to spin down and cool down. This results in an increase of the star's central density and a conversion of hadronic matter to quark matter in the dense, core regions of the star. The conversion is accompanied by relativistic bulk motions of the stellar fluid and causes a very efficient emission of GWs. Numerical calculations have shown that the GWs are emitted in the f-mode frequencies and carry energy as much as 10^{52}ergs. With this large energy carried by the waves, phase-transition events can be detectable in the galactic volume [5]. Similar events should be looked for in LMXBs as well; in these systems, it is the mass accretion that can trigger the transition and lead to considerable GW emission [8].

In compact binary coalescences, it is usually assumed that the final product after the merger is a black hole. But the prompt black-hole formation is not certain; especially in binaries with low-mass compact-star components, it will critically depend on the equation of state of high-density matter. There are numerical simulations showing that a hypermassive compact star can be formed [24, 23]. This object will most likely pulsate in its nonaxisymmetric fundamental modes until it eventually collapses to a black hole.

Such simulations show that the low-frequency inspiral chirp GW signal will be followed by a merger and by a high-frequency ring-down burst signal. In case a hypermassive compact star is formed, the signal will have a dominant frequency in the range 2-3kHz; in case of a prompt black-hole formation it will have even higher frequency. The amplitude of the ring-down signal will be large enough to be detectable from distances up to 50Mpc. We expect one binary compact-star coalescence per year at this distance while the detection rate of such events is estimated to be 0.4 to 400 per year with advanced interferometers [21].

2   Detectors

During the S5/VSR1 data-taking run five GW detectors were operational. The three LIGO detectors [1] started their Science Run 5 (S5) in November 2005, and the GEO 600 detector [2] joined the S5 run in January 2006. The Virgo detector [3] began its Virgo Science Run 1 (VSR1) in May 2007. All five instruments took data together until the beginning of October 2007.

In the years 2009-2010, data were taken for the sixth LIGO science run (S6) and for the second and third Virgo science runs (VSR2 and VSR3). During this period, the LIGO laboratory operated two 4km detectors: H1 at the Hanford observatory at Washington, USA and L1 at the Livingston observatory at Louisiana, USA; the Virgo Collaboration operated the Virgo V1 detector at Cascina, Italy. The S6/VSR2-3 runwas held from 2009 July 7 to 2010 October 20. For Virgo VSR2 started on 2009 July 7 and ended on 2010 January 8 to allow for an upgrade. Virgo resumed with VSR3 on 2010 August 11 and ended on 2010 October 20.

pair	time-slide (years)	zero-lag (days)
VH	73.9	89.9
VL	65.6	79.8
HL	73.1	89.3

Table 1: Time-slide (in years) and zero-lag (in days) lifetimes for the three pairs of our network. Only periods after data quality category 2 are taken into account.
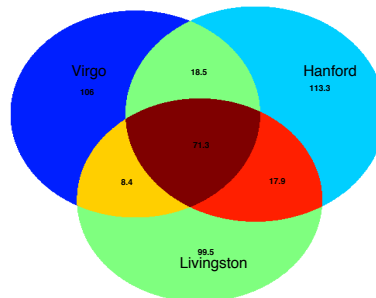

Figure 1: Venn diagram of lifetimes (in days) of different networks available for the current detection search (cf. Table 1).

3 Methodology

3.1 Template bank

Ring-down signals are damped sinusoids:

$$h = \sin\left(2\pi f t\right) e^{-\pi f t/Q} = \sin\left(2\pi f t\right) e^{-t/\tau} \tag{4}$$

where t is the time, f is the frequency, Q is the quality factor, and τ is the damping time ($Q = \pi f \tau$).

f-modes of compact stars with cold equations of state have frequencies, 1.5kHz $< f <$ 4kHz and damping times, 100ms $< \tau <$ 400ms, [4, 6]. Their quality factors are $900 < Q < 1800$. We cover the $f - Q$ parameter space with a set of 1695 templates. Any ring-down in this parameter space matches more than 90% with one of our templates (Fig. 2).

3.2 Trigger generation

With each template $h(t) == \sin\left(2\pi f t\right) e^{-\pi f t/Q}$ we match-filter the data $x(t)$. Practically, we calculate the Fourier transforms $\tilde{h}(f)$ and $\tilde{x}(f)$ of the template and the data, respectively, and then we calculate the signal-to-noise ratio (SNR=SNR(t)):

$$\text{SNR} = \frac{1}{N} \int \frac{\tilde{h}^*(f)\tilde{x}(f)}{S(f)} e^{2\pi i f t} df \tag{5}$$

where $S(f)$ is the power spectral density and N is a template normalization factor:

$$N^2 = \int \frac{|\tilde{h}(f)|^2}{S(f)} df \tag{6}$$

Whenever an SNR is greater than a detection threshold a pixel is generated and the parameters of the pixel are recorded. Each pixel is characterized by its time and by the pair of parameters (f, Q) of the generating template. Usually, a template gives sets of pixels very closely spaced in time; these sets of pixels are clustered together to produce a single-template finite-duration trigger. For our search, the detection threshold is set to 5, and, for each trigger, we save its (maximum) SNR, its "start time", its "end time" and its "maximum time" (that is, the time of the pixel with the maximum SNR). We also save the frequency of the template (the corresponding Q factor can be easily recovered each time as the fs and Qs are in a 1-1 correspondence and thus it is not necessary to record its value, cf. Figure 2).
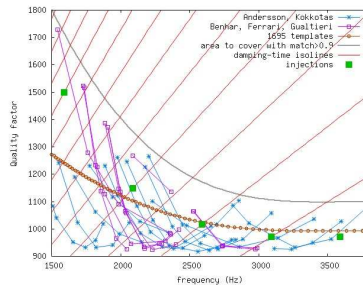

Figure 2: The frequency-quality factor (f-Q) parameter space of f-modes as predicted by Andersson & Kokkotas 1998, and Benhar, Ferrari & Gualtieri 2004 [4, 6]. We cover it with a bank of 1695 templates so as to have a minimum match of 90%. Most compact stellar models are located in the lower-right part of this figure and have damping times $\sim$ 100ms. Less relativistic models, on the other side, have damping times $\sim$ 400ms. We inject ring-downs of specific (f, Q) values but we try to spread them across the parameter space.
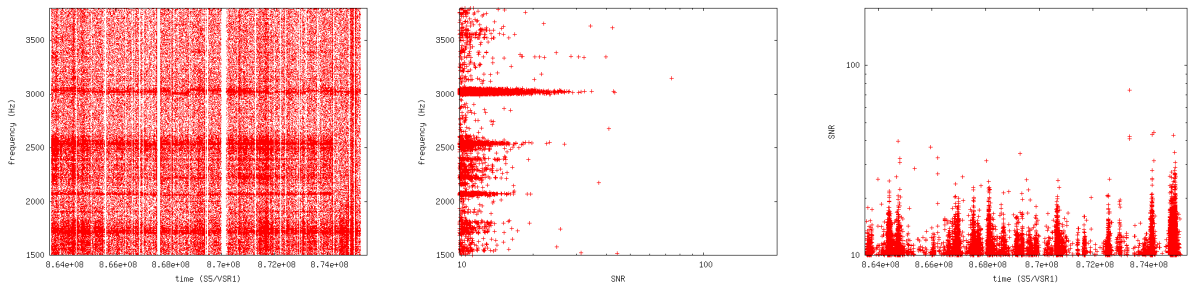

Figure 3: Triggers for the Virgo detector. Time-frequency (left), SNR-frequency (middle) and time-SNR plot (right). There is an excess of (loud) triggers at the frequency bands 2990Hz $< f <$ 3060Hz, 2520Hz $< f <$ 2550Hz and 2060Hz $< f <$ 2080Hz. These bands are vetoed (they are not taken into account).

3.3   Clustering

Whenever a ring-down signal is present in the data, one or more templates are excited. The louder the signal is, the more templates give large SNRs above the detection threshold of 5. When nearby templates are triggered around the same time, they are probably due to the same signal. Thus, we cluster single-template triggers together to produce multi-template triggers. Each multi-template trigger is characterized by its maximum-SNR pixel but has also a duration and a bandwidth.

In the left plot of Figure 3, we show the time-frequency map for the Virgo detector. An excess of loud triggers at specific frequencies ($2990\mathrm{Hz} < f < 3060\mathrm{Hz}$, $2520\mathrm{Hz} < f < 2550\mathrm{Hz}$ and $2060\mathrm{Hz} < f < 2080\mathrm{Hz}$) is clearly visible. This is also clear in the SNR-frequency plot in the middle of the figure. Also, there are time periods with an increased trigger rate (right plot).
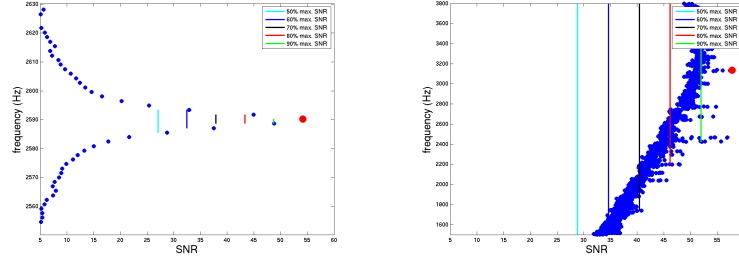

Figure 4: The response of the template bank to a ring-down injection (left) and a non ring-down signal (right). Although the two triggers have very similar maximum SNRs, there is a clear difference between the two cases. The energy of a ring-down is well located in frequency; only templates around the injected frequency are triggered above the detection threshold. On the other hand a spike glitch, for example, triggers a large number of templates to high SNRs. This search looks for signal of the former response and signals of the later response are therefore vetoed.

3.4   Signal-based vetoes

We search for specific signal waveforms, that is ring-downs (4), and this is already implied as we make a match-filtered search (with ring-down templates). But, that is not enough and we can do even more than that. Other, non ring-down, signals may have large energy content in high frequencies and may excite considerably our templates. But, most likely, they will excite the bank in a very different way which may be identified and vetoed. In other words, we can discriminate between ring-down and other (high-frequency) signals by checking the response of the template bank and by using signal-based vetoes.

When a ring-down signal is present in the data the template bank responds in a specific way. If a different signal is present in the data (for instance, a high-frequency sine Gaussian or a signal with two different frequencies) the template bank responds in an unexpected way and thus we can reject it, as it is not what we are looking for.

In Figure 4, we show the response of our template bank to a ring-down injection (left) and a non ring-down signal (right). Although the two triggers have very similar maximum SNRs (~ 60), there is a clear difference between the two cases. The energy of a ring-down is well located in frequency; only templates around the injected frequency are triggered above the detection threshold. On the other hand, a shorter (for example, a spike) signal excites many more templates with comparable SNRs. A ring-down dedicated search vetoes triggers which behave in this unexpected way.

3.5   Background estimation

To estimate the significance of candidate GW events, and to optimize event selection cuts, we need to measure the distribution of events due to background noise. With a multidetector analysis one can create a sample of background noise events and study its statistical properties. These samples are created by time-shifting data of one or more detectors with respect to the others by unphysical time delays (i.e. much larger than the maximum time-offlight of a GW signal between the detectors). Any triggers that are coincident in the time-shifted data cannot be due to a true gravitational-wave signal; these coincidences therefore sample the noise background. Background estimation is done separately for each pair, using 300 shifts of 6 seconds.

3.6   Efficiency estimation

To estimate the efficiency of our pipeline we inject ring-down signals in the data. Then we check how many of these injected signals are recovered (how many pass the tuning thresholds). This number depends on the parameters of the injected signal (mainly on the frequency), on the signal strength (which is measured by the hrss) and on its polarization.

4 Results

4.1 Tuning

We tune the pipeline by comparing the coincident triggers from time-slides and from injections. We apply thresholds to reduce the background rate to a target, pre-defined false-alarm rate (FAR). There are many sets of thresholds to do that; not all of them result in the same efficiency, though. Among all the possible sets of thresholds that give us the desired FAR, we choose the one that provides major sensitivity.

The FAR for this search is pre-defined to be 1 event in approximately 7 years. This tranlates to less than $5 \cdot 10^{-9}$Hz. The detection efficiency is evaluated through the detection integral:

$$I = 10^{-63} \int_0^\infty dh h^{-4} \epsilon \tag{7}$$

where $\epsilon(h)$ is the efficiency in detecting a signal of strength h (at the earth). The integral assumes a spherical, isotropic distribution of sources.

For the VHL (triple or) network, the background lifetime is $\sim$213 years (see Table 1). In order to have the target FAR, we ask for 30 time-slide coincidences above the thresholds.

We start by applying two thresholds per pair, thr_1 and thr_2, on the SNRs of the two detectors, SNR_1 and SNR_2, respectively. Subsequently, each pair's surviving time-slide coincidences are subject to a third threshold, thr_{12}, on the product of the two SNRs, $SNR_1 \cdot SNR_2$. Table 2 summarizes the set of thresholds and the resulting data reduction.

pair	thr_1	thr_2	bkg	zero	thr_{12}	bkg	zero
VH	6.5	6.2	37	0	47.8	4	0
VL	5.7	6.0	529	1	47.9	5	0
HL	6.0	5.4	933	6	42.5	21	0

Table 2: Set of thresholds and resulting data reduction. After thr_1 and thr_2, 1499 background and 7 foreground events remain. The additional thr_{12} ensures the target FAR of 30 time-slide coincidences for the (VH or VL or HL) network. At this FAR, no zero-lag coincidences survive. This set of thresholds maximizes the detection integral (7).
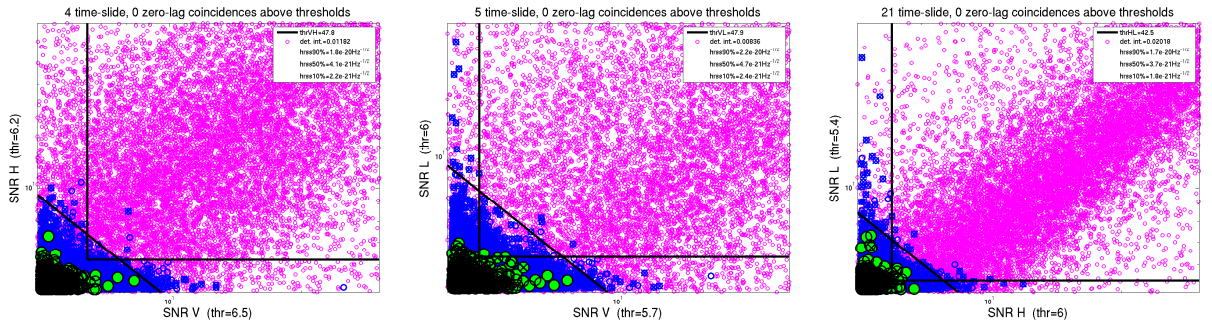

Figure 5: Tuning and results for the VH (left), VL (middle) and HL (right) pairs. The circles represent time-slide coincidences (blue), zero-lag coincidences (green) and injections (magenta). The lines show the chosen thresholds (cf. with Table 2).

4.2 GW candidates

Now, let's have a look at the zero-lag coincident events. We find no such events above the chosen thresholds. As one can see in Figure 5, all the zero-lag coincidences (green circles) are far below the SNR thresholds. This means they are statistically not significant. We now proceed to set upper limits based on the non-detection statement. We search for the loudest zero-lag event in the data. For this, we assign a detection statistic to each time-slide, zero-lag and injection coincidence that passes thr_1 and thr_2 in each pair. The statistic is defined to be the product of the SNRs of the two detectors weighted by the relevant detection threshold, thr_{12}:

$$\text{detection statistic} = \frac{SNR_1 \cdot SNR_2}{thr_{12}} \tag{8}$$

We, then, merge time-slide and zero-lag coincidences from all pairs together and produce the cumulative histogram of Figure 6. From that figure, we see that the FAR of the loudest event is approximately 277 events in 213 years. This event happens at the HL pair and it has a detection statistic equal to 0.87. At the loudest event's detection statistic, which corresponds to $thr_{12} = 41.4, 41.5$ and 36.8 for the VH,VL and HL pairs respectively, we calculate the efficiency of the pipeline. The efficiency depends on the ring-down waveform (especially on its frequency) and on its polarization. Table 3 summarizes the results.

4.3 Astrophysical interpretation

Assume a spherical and isotropic distribution of standard-candle sources (for example, glitching compact stars) emitting gravitational waves with energy E at a rate density R (number per time per volume). The expected number of detections, N_{det}, given the network efficiency ϵ (for injections without any inclination-angle dependence) and the observation time T is [19]:

$$N_{\text{det}} = 4\pi RT \left(h_{\text{rss}} r_0 \right)^3 \int_0^\infty dh h^{-4} \epsilon \tag{9}$$

The lack of detection candidates in the S5/VSR1 data set implies a 90% confidence upper limit on rate density R of:

$$R_{90\%} = \frac{2.0}{4\pi T \left(h_{\text{rss}} r_0 \right)^3 \int_0^\infty dh h^{-4} \epsilon} \tag{10}$$

For sources with amplitude h_{rss}, with characteristic frequency f_0, at a fiducial distance r_0:

$$h_{\text{rss}} r_0 = \sqrt{\frac{GE}{c^3}} \left(\pi f_0 \right)^{-1} \tag{11}$$

Combining equations (7), (10) and (11):

$$R_{90\%} = 10^{-63} \left(\frac{GE}{c^3} \right)^{-3/2} \frac{\pi^2 f_0^3}{2TI} \simeq 2 \cdot 10^{-3} \frac{f_{\text{kHz}}^3}{I} \text{yr}^{-1} \text{pc}^{-3} \simeq 0.4 \text{yr}^{-1} \text{pc}^{-3} \tag{12}$$

For the S5/VSR1 run, $T \simeq 0.7$yr. In the last equality, we assume $E = 10^{42}$ergs and $f_0 = 2090$Hz. For this frequency, and a linearly polarized ring-down signal, Table 3 gives $I = 0.035$.

The Vela pulsar, located $\simeq 300$pc far from the Earth, glitches -roughly- once every 2.5 years. The glitch rate density, extrapolated by this observation, is $\sim 3.5 \cdot 10^{-9}$yr^{-1}pc^{-3}.
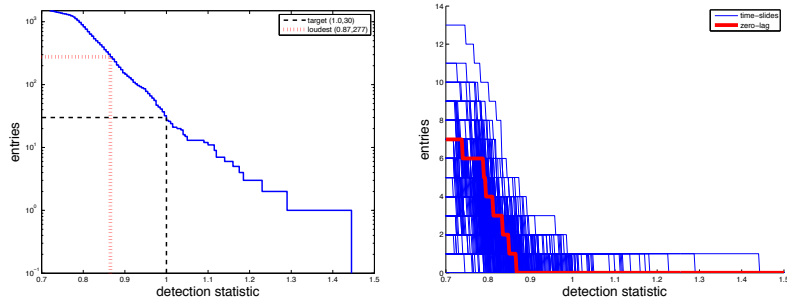

Figure 6: Left: Cumulative histogram of the detection statistic (blue solid line). Its detection threshold (black dashed line) ensures a low false-alarm rate of 30 events in 213 years. The loudest event (red dotted line) is found at a much higher false-alarm rate (277 events in the same background lifetime). Right: Cumulative histograms per time-slide (blue) and for zero-lag (red).

	1590Hz	2090Hz	2590Hz	3090Hz	3590Hz
RDL	0.087	0.035	0.020	0.012	0.008
RDC	0.066	0.032	0.017	0.010	0.007

Table 3: Detection integrals for ring-downs with different frequencies (1590Hz-3590Hz) and different polarizations (linearly polarized, RDL, and circularly polarized, RDC).
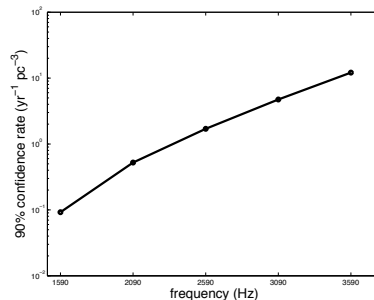

Figure 7: Rate limit per unit volume at the 90 % confidence level for a linearly polarized ring-down standard-candle with $E = 10^{42}$ergs.
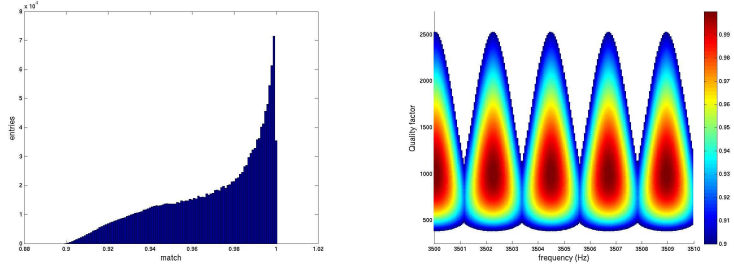
Figure 8: Any injected ring-down with (f, Q) parameters drawn from our parameter space matches at least by 90% with at least one template from our bank (left). A template at some frequency practically is sufficient for all the possible Q values. Our template bank is essentially one-dimensional (right).

A   Template bank details

The match between two ring-down signals $h_1 = \sin(2\pi f_1 t)e^{-\pi f_1 t/Q_1}$ and $h_2 = \sin(2\pi f_2 t)e^{-\pi f_2 t/Q_2}$ is defined as their normalized inner product:

$$\frac{\int h_1 h_2 dt}{\sqrt{\int h_1^2 dt \int h_2^2 dt}} \tag{13}$$

For a large set of ring-down signals, with (f, Q) parameters drawn from our target parameter space (Figure 2), we have calculated their minimum match with our template bank. We have found that for all signals, there exists at least one template from our bank that matches more than 90%. This is shown in Figure 8. It is easy to see that the match maximizes (equals to unity) when the (f, Q) parameters coincide with those of a template from our bank.
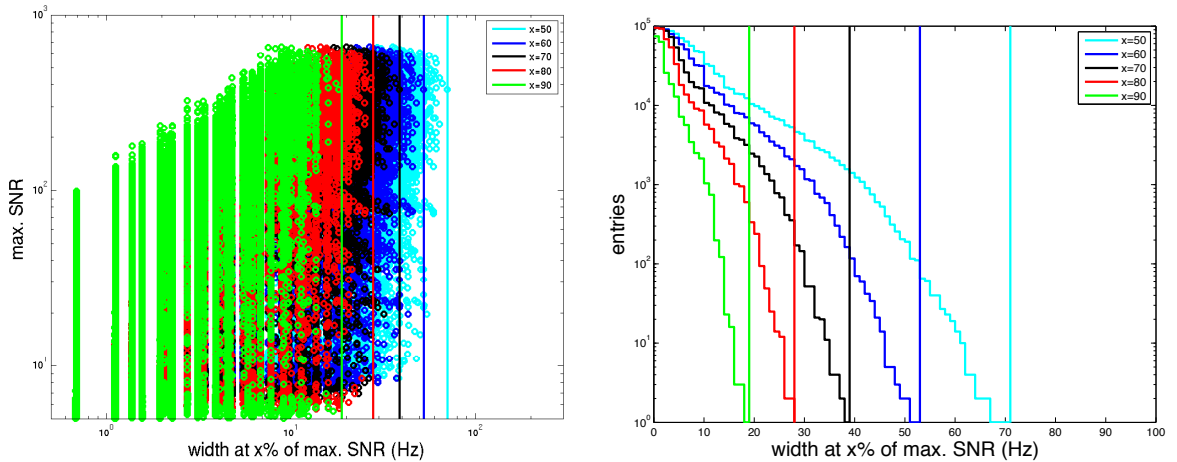
B   Signal-based vetoes details

Figure 9: By injecting (~ 100000) ring-downs, we set cuts on their bandwidths at various SNR levels. In the left part of the figure, each circle represents an injection and appears in five different colors. A cyan circle gives the (band-)width of the injection at 50% of the maximum SNR, a red circle gives the width at 60% of the max. SNR, and so on. On the right part of the figure, we show the corresponding cumulative histograms. We see, for example, that all injections have a width less than 19Hz at 90% of their maximum SNR or that their full width at half their maximum (FWHM) is less than 71Hz. The way these cuts work is explained and shown in Figure 4. More details on the final values of these cuts can be found in Table 4.

We inject a large set of ring-downs (order 100000 injections) of various frequencies, in all three detectors (H,L and V) with varying (hrss) strengths and with both polarizations (linear and circular). For each injection, we find its widths at various SNR levels (from 50% to 95%). We then form Table 4 taking care to include all injections.

x% of max. SNR	50	55	60	65	70	75	80	85	90	95
width (Hz)	71	62	53	46	39	35	28	23	19	12

Table 4: The values of the signal-based veto cuts. (Cf. with Figures 4 and 9.) Example: if a trigger with a maximum SNR of 100 has a width greater than 71Hz at the SNR-level of 50 (in other words, if templates giving SNRs over 50 are more than 71Hz apart) this trigger is considered **not** a ring-down and is vetoed.